Alteration of Atmospheric Solar Absorption by Clouds: Simulation and Observation

ZHANQING LI*

Canada Centre for Remote Sensing, Ottawa, Ontario, Canada

LOUIS MOREAU

Intera Information Technology Limited, Ottawa, Ontario, Canada

(Manuscript received 10 May 1995, in final form 20 October 1995)

ABSTRACT

This study investigated theoretically and experimentally two parameters employed in recent attempts to address cloud absorption anomaly. One is the ratio, R, of shortwave cloud radiative forcing (CRF) at the surface to that at the top of the atmosphere (TOA), and another is the slope, s, of the regressional relationship between TOA albedo and atmospheric transmittance. The physics and sensitivities of the two parameters were first examined by means of radiative transfer modeling. Neither R nor s is a direct measure of cloud absorption. However, R can indicate the effect of clouds on the atmospheric absorption of solar radiation, if clear-sky condition remains the same. A value of $R > 1$ implies clouds warm the atmosphere, while the converse is true for $R < 1$. Model simulations suggest that both R and s are sensitive to many factors, especially cloud height and surface condition. Nonetheless, modeled R rarely exceeds 1.25, and modeled s is generally less than -0.7, except for bright surfaces. The slope s can be related to R under certain conditions. Observational values of R and s were then determined using four years worth of global satellite and ground-based monthly mean solar flux data from the Earth Radiation Budget Experiment (ERBE) and the Global Surface Energy Balance Archive (GEBA). The ratio R is highly variable with both location and season and also shows strong interannual variability. Low to moderate values of R, attainable by plane-parallel radiative transfer models, tend to occur over relatively clean regions. Large values of R appear to associate with either heavy pollution in the midlatitudes or frequent occurrence of biomass burning in the Tropics. The large values of R in the Tropics are less reliable than the low and moderate R in the midlatitudes. While this study does not rule out cloud absorption anomaly, it does indicate, however, that its magnitude (if it exists) is not as large, and its occurrence not as widespread, as suggested in some recent reports.

1. Introduction

Cloud and radiation play key roles in weather and climate. The two variables interact strongly, posing two scientific questions as to how clouds modify radiation and, in return, how radiation influences the evolution of clouds. Although the former is a relatively straightforward problem and has been tackled for a long time, some fundamental issues have still not been fully resolved. Absorption of solar radiation by clouds is the most basic to understand cloud–radiation interactions, which is, unfortunately, still haunting to atmospheric scientists (Stephens and Tsay 1990; King 1993). For over 40 years, there have been reported observations of cloud absorption that exceed theoretical estimates (Fritz 1951; Robinson 1958; Reynolds et al. 1975; Foot 1988). This phenomenon is often referred to as the cloud absorption anomaly (Wiscombe et al. 1984). On the other hand, overall agreements between observations and calculations have also been reported (Slingo et al. 1982; Herman and Curry 1984; Hignett 1987; Rawlins 1989). Spectral comparisons tend to show better agreements at visible wavelengths than in the near-infrared (Stephens and Platt 1987).

Strictly speaking, one can only claim an absorption anomaly if his/her observations do not agree with the results of the state-of-the-art radiative models supplied with accurate and complete data for input parameters or if the discrepancies are so large that no matter what models and input parameters are used, agreements cannot be achieved. By these standards, some claimed findings of the cloud absorption anomaly in the literature may no longer be qualified. To date, most observational studies on cloud absorption were based on in situ aircraft measurements. For horizontally homogeneous clouds, solar flux absorbed by clouds is simply equal to the difference between simultaneous and collocated measurements of net radiative fluxes observed at the upper and lower bounds of the cloud layer. Often the difference is far more noisy than the original flux

Corresponding author address: Dr. Zhanqing Li, Canada Centre for Remote Sensing, 588 Booth Street, Ottawa, ON K1A OY7, Canada.
E-mail: li@ccrs.emr.ca

measurements, owing to the loss in significant digits. For inhomogeneous clouds, determination of the flux absorbed in a cloud layer is complicated by the horizontal leakage of photons. After a careful treatment of this effect, Hayasaka et al. (1995) were able to bring a substantial disagreement to a good agreement between observed and calculated cloud absorptance. Besides, one should not overlook the uncertainties in the input parameters required for radiative transfer calculations, when comparing theoretical results with observations. It is likely that the errors resulting from inaccurate input parameters are comparable to, or even larger than, the discrepancies reported thus far between observed and computed cloud absorption.

However, these concerns seem uncalled for from some recent studies that proposed that the signal of cloud absorption anomaly may exceed by far the uncertainties associated with these factors (Ramanathan et al. 1995; Cess et al. 1995; Pilewskie and Valero 1995). Notwithstanding different approaches, they all attempted to relate cloud absorption with the ratio, R, of shortwave cloud radiative forcing (CRF) at the surface to that at the top of the atmosphere (TOA). From different types of observations (spaceborne, airborne, and ground based), they ended up with similar values for R around 1.5, while conventional radiative transfer models tend to produce R near unity. In fact, Pilewskie and Valero (1995) found even higher R, but they claimed that their value was consistent with 1.5. In order for radiative transfer models to produce $R = 1.5$, the values of cloud specific absorption (1 minus single scattering albedo) need to increase by a factor of 40 relative to those inferred from aircraft measurements (King et al. 1990), baring significant absorption in the visible spectral region (Chou et al. 1995). As is further reinforced in this study, $R = 1.5$ is certainly beyond the reach of any conventional radiative transfer model even with very extreme conditions pertinent to cloud, atmosphere, and surface that facilitate large R.

If $R = 1.5$ is universally true, contemporary radiation models used both in current general circulation models (GCMs) and in the retrieval of surface solar radiation budget from satellite measurements could overestimate the global and annual mean solar flux absorbed at the surface by about 25 W m^{-2} due to underestimation of cloud absorption alone (Cess et al. 1995). In addition, shortwave models also suffer considerable disparity among themself (Fouquart et al. 1991) and with respect to satellite-based estimates (Li and Barker 1994) under clear sky conditions. For example, many conventional schemes for water vapor absorption tend to underestimate atmospheric absorption relative to the benchmark results of line-by-line calculation. Underestimation of atmospheric absorption is also caused by neglect of absorbing aerosols in many models including GCMs. The amount of such an underestimation could be comparable to, or even larger than, 25 W m^{-2} on global average (Li and Barker 1994; Barker and Li 1995). Therefore, if these findings are all correct, GCMs could have underestimated atmospheric absorption by up to 50 W m^{-2}, which is a 100% relative error for some GCMs and more than 15 times the radiative effect of doubling CO_2 simulated by GCMs (Cess et al. 1993)! However, direct comparisons between GCM simulations and surface observations suggested an overall discrepancy in the neighborhood of 25 W m^{-2} (Garratt 1994; Wild et al. 1995).

In view of the magnitude of the discrepancy and the fundamental nature of the problem, Wiscombe (1995) remarked that the field of atmospheric solar radiation studies has been caught "napping in basic research" but "wide awake in developing applications." The present study attempts to shed a light on this cloudy issue with the aid of comprehensive radiative transfer modeling and analyses of a large volume of data from both satellite and surface observations. The physics of the two parameters employed in this study is discussed in section 2. Section 3 examines their sensitivities to cloud, surface, and atmospheric conditions. Section 4 describes the data used for experimentally determining these parameters. Their values and variations are analyzed in section 5. Section 6 summarizes the investigation. A brief discussion of the preliminary work has been reported in Li et al. (1995a).

2. Parameters

The two parameters employed in this study are the same as those used by Ramanathan et al. (1995) and Cess et al. (1995). Although neither of these parameters directly measure cloud absorption, they could be valid to reveal cloud absorption anomaly if, *and only if,* the magnitude of the anomaly is as large as they claimed.

The cloud radiative forcing ratio R is defined as

$$R \equiv \frac{\mathrm{CRF_{SFC}}}{\mathrm{CRF_{TOA}}} = \frac{F^{\mathrm{all}}_{\mathrm{SFC}} - F^{\mathrm{clr}}_{\mathrm{SFC}}}{F^{\mathrm{all}}_{\mathrm{TOA}} - F^{\mathrm{clr}}_{\mathrm{TOA}}}, \quad (1)$$

where F denotes shortwave net fluxes for all sky (all) and clear sky (clr) conditions at the TOA or surface, as indicated by the subscripts. Note that CRF is also modified by factors other than clouds, such as surface and atmospheric conditions and solar zenith angle (SZA) (Rossow and Zhang 1995).

Following the definition of (1), Ramanathan et al. (1995) obtained R for the western equatorial Pacific warm pool (10°S–10°N, 140°–170°E). In their study, all-sky and clear-sky TOA fluxes were derived directly from Earth Radiation Budget Experiment (ERBE) measurements, whereas surface fluxes were estimated. All-sky surface net shortwave fluxes were determined as the residual term in the surface heat balance equation that relates surface net heat flux to surface net shortwave and longwave radiative fluxes and latent and sensible heat fluxes. Clear-sky surface net fluxes were inferred from ERBE clear-sky TOA fluxes using an in-

version algorithm (Li et al. 1993a). CRF_{SFC} and CRF_{TOA} were estimated to be -100 and -66 W m^{-2}, respectively, leading to $R \approx 1.5$. Our method of determining R differs from theirs only in the derivation of all-sky surface net shortwave flux. We compute it from the observed surface insolation and inferred surface albedo, as detailed later.

To reveal the physical meaning of R, CRF_{SFC} is rewritten as

$$CRF_{SFC} = CRF_{TOA} - CRF_{ATM}, \quad (2)$$

where CRF_{ATM} is atmospheric CRF that defines the difference in atmospheric absorption for all-sky and clear-sky conditions. Substituting (1) into (2) and rearranging gives

$$CRF_{ATM} = (1 - R)CRF_{TOA}. \quad (3)$$

Since in general, $CRF_{TOA} < 0$ (Ramanathan et al. 1989; Harrison et al. 1990), $R > 1$ and $R < 1$ imply, respectively, that clouds enhance and reduce atmospheric absorption relative to clear-sky absorption. When $R = 1$, cloud absorption equals exactly the reduction in absorption by gases and aerosols beneath cloud due to reduced transmittance, less the slight enhancement in absorption by gases and aerosols above cloud due to increased reflectance. Hence, R is not a direct measure of cloud absorption, but rather a measure of the changes in absorption of solar radiation by the entire cloudy atmospheric column relative to its clear counterpart. As is manifested from the sensitivity tests presented in the following section, R is not only modified by the optical properties of clouds but also by the solar zenith angle, cloud height, vertical distribution of water vapor and aerosol, and surface condition. Therefore, one cannot unambiguously attribute the changes in R to the changes in the effect of clouds on atmospheric absorption, unless the parameters other than cloud remain invariant. These limitations do not, however, negate the basic conclusion of Ramanathan et al. (1995), as the collective effect of these parameters never renders R larger than 1.25 (see next section).

Cess et al. (1995) related the slope s in the relationship between coincidental TOA albedo α_p and atmospheric transmittance t_a to CRF ratio R by

$$R = -\frac{1 - \alpha_s}{s}, \quad (4)$$

where α_s denotes surface albedo. Note that the sign of s in (4) is opposite to that used in Cess et al. (1995). There are several advantages using s over R. First, there are more observations of surface insolation than surface net flux. Second, no clear-sky data are required as long as changes in cloud condition are large enough to ascertain a meaningful regression between α_p and t_a. Third, inference of clear-sky surface net flux and albedo is circumvented. By analyzing collocated satellite and surface measurements at various locations, Cess et al. (1995) found that the values of s are always close to 0.6, whereas GCMs produce R near 0.8, which are equivalent to $R = 1.4$ and 1.0, respectively, for $\alpha_s = 0.17$ (Cess et al. 1995). However, it must be pointed out that (4) is not a universal relationship. There are two assumptions for (4) to be valid. First, surface albedo does not depend on cloud, that is, clear-sky surface albedo is the same as for all-sky albedo. Since the presence of clouds alter the spectral distribution of incoming solar energy, this assumption may be violated when surface albedo depends strongly on wavelength. Second there is a universal linear relationship between TOA albedo and atmospheric transmittance. As demonstrated in the next section, this assumption can be readily invalidated if no constraints are applied to the regression. In essence, the slope of the relationship is modified by many factors such as surface albedo, solar zenith angle, cloud height, etc.

3. Sensitivity

a. Model

The radiative transfer model employed for the sensitivity tests of R and s is a doubling–adding code that was described in detail by Masuda et al. (1995). The model has 120 wavelength bands spanning from 0.25 to 25.0 μm. It was validated against line-by-line codes under both clear and cloudy conditions and showed good agreements. Radiative transfer calculations were done by applying the model to a plane-parallel, vertically inhomogeneous atmosphere divided into eight homogeneous layers (0–1, 1–2, 2–4, 4–6, 6–9, 9–13, 13–25, and 25–100 km). The model accounts for the radiative effects of air molecules, clouds, water vapor, ozone, and aerosols. Clouds may be placed in any layer, while the bulk of aerosol is contained in the boundary layers below 2 km. Vertical distributions of water vapor, ozone, CO_2, and other trace gases are given by the model atmospheres of McClatchey et al. (1972). Absorptance and transmittance at each 5-cm^{-1} spectral interval were computed by the LOWTRAN 7 band model for absorption due to water vapor and by the model of Braslau and Dave (1973) for absorption due to other gases. The band-mean transmittances were then used to determine the weights and extinction coefficients in an exponential sum fit for up to seven terms. Different types of clouds (stratus St, cumulus Cu, stratocumulus Sc, nimbus Nb) and a moderately absorbing continental aerosol (CON-I) of varying optical thicknesses were considered. The optical properties of these clouds, differentiated by their droplet size distributions, were taken from Stephens (1978), and those for the aerosol were from WCP-112 (1986). Four surface types were used: cropland, desert, snow, and water. These surfaces are distinct in broadband and spectral albedo and in their dependencies of albedo on wavelength and solar zenith angle (Masuda et al. 1995). Extraterrestrial solar

spectrum was taken from Iqbal (1983). For each atmosphere–surface combination, calculations were made at 11 SZAs, including 89.4°, 86.9°, 82.2°, 76.1°, 68.6°, 60.0°, 50.6°, 40.5°, 30.1°, 19.3°, and 8.5°. Daily mean fluxes were also computed by integrating instantaneous fluxes at specific solar zenith angles from sunrise to sunset for particular latitude and time of the year (Li and Garand 1994).

b. *Sensitivities of R*

It is seen from (1) that R is determined by all-sky and clear-sky solar fluxes at both the TOA and surface. Clear-sky fluxes were computed for the same atmospheric and surface conditions as the computation of all-sky fluxes. Figure 1 shows the variation of R with cloud optical thickness τ. Except for a minor fluctuation at small τ, R remains almost invariant for $\tau > 10$. The ratio R is also found (not shown here) to be independent of cloud amount when fluxes for partial cloudiness were computed by weighting the clear and overcast fluxes by their respective fractions. Therefore, overcast clouds with an ad hoc selection of $\tau = 40$ are used in subsequent sensitivity tests. Figure 2 shows the dependence of R on SZA for St-I clouds at four different heights (0–1, 1–2, 4–6, 9–13 km). The St-I cloud has a mode radius (corresponding to the maximum number of drops) of 3.5 μm, liquid water content of 0.22 g m^{-3}, and drop number concentration of 440 cm^{-3} (Stephens 1978). In general, R decreases with increasing SZA at varying rates depending on cloud height: faster for higher clouds than for lower clouds. The dependencies of R on both SZA and cloud height are caused primarily by varying the amount of water vapor and aerosol below the cloud layer. With the presence of clouds, many photons are reflected back to space and thus deprived a chance of being absorbed by the absorbers below the clouds. The higher the cloud, the more the low-level absorbers are shielded, and thus the smaller the amount of solar energy absorbed in the atmospheric column and the lower the value of R. Therefore, depending on cloud height as well as SZA, clouds may warm ($R > 1$) or cool ($R < 1$) the atmosphere relative to clear-sky absorption, as is shown in Fig. 2. Sensitivities of instantaneous R were also studied by Chou et al. (1995). Their results agree qualitatively with ours except they tended to produce R slightly less than 1 due to the use of different cloud model and radiative transfer model.

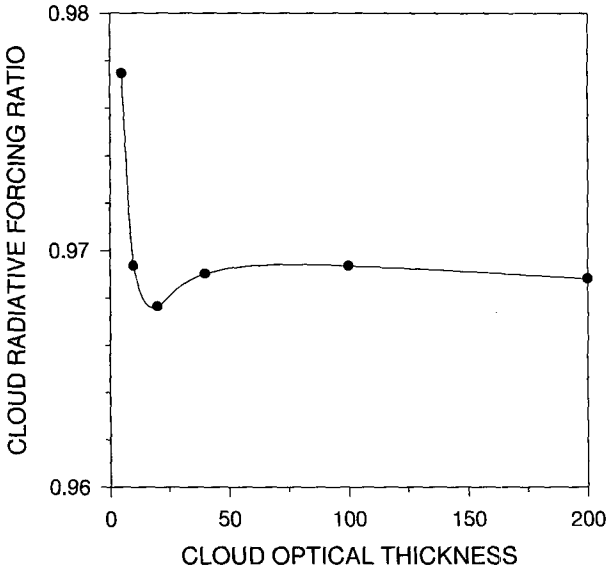

FIG. 1. Diurnal-mean ratios of surface to TOA shortwave cloud radiative forcing (R) simulated for July at 30°N with St-I cloud of varying optical thickness situated at 2–4 km. A midlatitude summer atmosphere with a CON-I aerosol of optical thickness 0.225 over cropland is used. Diurnal-mean R is computed from the diurnal-mean CRF at the surface and TOA, which are simulated from daily mean fluxes under clear and cloudy conditions.

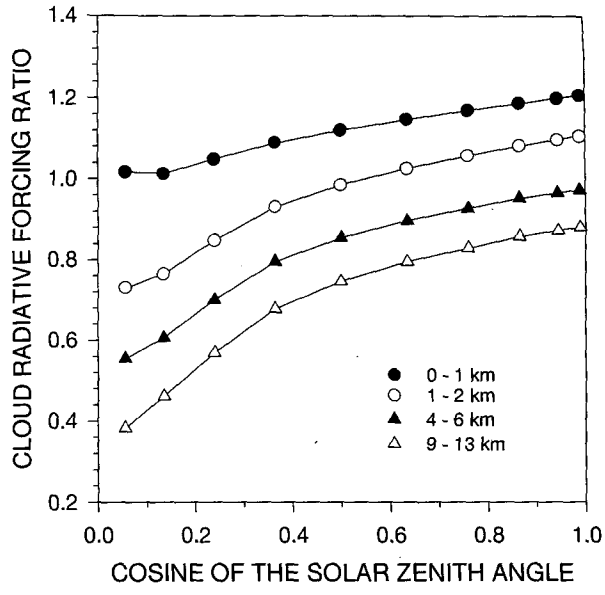

FIG. 2. Modeled R as a function of cosine of the solar zenith angle for a St-I cloud of optical thickness 40 located at different altitudes. The same atmospheric and surface conditions as in Fig. 1 are employed.

In order to lessen the dependency of R on SZA and to compare with observational results, diurnal mean values of R are employed in the following discussions. Diurnal mean R was computed from the diurnal mean surface and TOA CRF that were further determined from daily mean fluxes for clear and cloudy conditions. Although the plane-parallel model does not perform well at large solar zenith angles, the impact is minor on the daily mean fluxes due to low incoming solar energy. Figure 3 depicts the variation of diurnal mean R with cloud-top altitude, simulated for 30°N in July with St-I cloud of constant τ (40) and its base reaching the ground. The turning point, $R = 1$, takes place at a

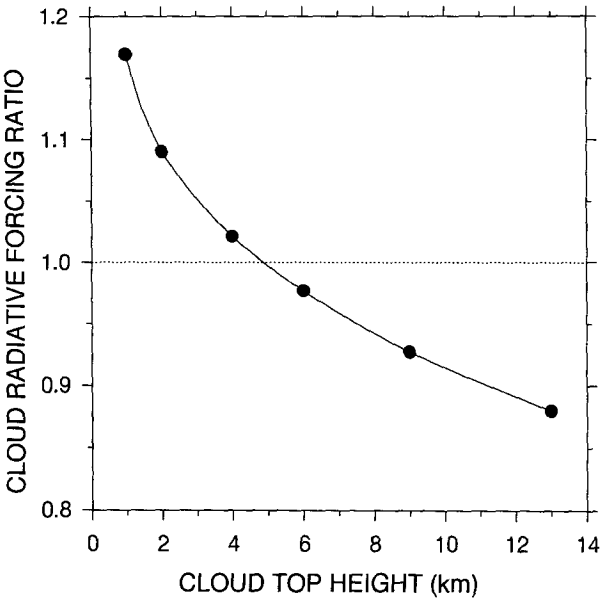

FIG. 3. Variation of diurnal-mean R as a function of cloud-top altitude. The same atmospheric, cloud, and surface conditions as in Fig. 1 are employed except that cloud base is set to 0 km.

cloud-top altitude near 5 km. Clouds with their tops higher and lower than this altitude have opposite effects on the total atmospheric absorption of solar radiation. The turning point depends also on the altitude of cloud base. For instance, R diminishes from 1.08 to 0.97 when cloud base is elevated from the ground to 2 km for a fixed cloud top of 4 km. Increasing cloud-base altitude reduces the chance of photons being absorbed by low-level absorbers. Apart from cloud position, cloud microphysics exert an influence on R. The particle size distribution of cloud droplets modifies both single-scattering albedo and the scattering phase function and thus affects the column absorption and R. Table 1 delineates the values of daily mean R corresponding to four cloud types with different size distributions. The effective radius of cloud droplets increases from St-I to Sc-II to Cu and to Cb. Since the single-scattering albedo of cloud droplets decreases as their effective radius increases, the values of R increase with effective radius. Comparing Table 1 to Figs. 2 and 3, however, shows that R is more sensitive to cloud position than to cloud microphysics.

Aerosol may have a significant impact on R depending on its optical properties and distribution relative to cloud layer. For example, for a St-I cloud located 0–1 km with the midlatitude summer atmosphere containing CON-I (WCP-112) aerosol, diurnal mean R goes from 1.14 to 1.22 when the aerosol optical thickness increases from 0.056 to 0.45. Ninety percent of CON-I aerosol content is limited to 0–2 km. When the cloud is lifted to 2–4 km, the same change in aerosol optical depth reduces R from 1.02 to 0.94, although

TABLE 1. Diurnal-mean R simulated for July at 30°N for four cloud types with optical thickness 40 situated at 2–4 km. The midlatitude summer atmosphere with a continental aerosol of optical thickness 0.225 over cropland is used.

	Cloud type			
	St-I	Sc-II	Cu	Cb
Ratio R	0.97	1.00	1.01	1.07

total atmospheric absorption increases slightly. This is because clear-sky absorption augments more than cloudy-sky absorption when the aerosol optical depth increases. This demonstrates that R is not an absolute measure of total atmospheric absorption but rather a relative measure of cloudy-sky absorption versus clear-sky absorption. The interdependence of R on cloud height and water vapor is similar to that of aerosol.

Finally, the effects of surface type on R are investigated and the results are given in Table 2. Except for snow and ice, the dependence of R on surface albedo is weak for the range of surface albedos considered here. For snow and ice surfaces, the very low R (0.43) indicates that the addition of a cloud at 2–4 km deducts total atmospheric absorption considerably relative to the corresponding clear-sky case. Again this is because the cloud prevents many photons from reaching the underlying layer that houses most of the aerosol and water vapor. For clear skies, many photons would have traversed this lower layer and thus would have stood a larger chance of being absorbed. Conversely, R becomes 1.2 when the cloud is lowered to 0–1 km. This is because of increased photon pathlength and scattering events in the aerosol layer.

c. *Sensitivities of s*

Figure 4 shows the relationship between TOA albedo and atmospheric transmittance for varying SZA and St clouds with optical thickness between 0 and 40 over a cropland. The two variables have a good linear relationship except for the three largest SZAs greater than 80°. As the amounts of solar energy are very small for these SZAs, the relationship between diurnal-mean α_p and t_a is also highly linear with a slope similar to that

TABLE 2. Same as Table 1 except for St-I cloud over different surface types. The value of R for the snow–ice surface is obtained for January instead of July. Broadband surface albedos for April in 60°N are also included.

	Surface type			
	Snow	Desert	Crop	Water
Albedo	0.91	0.40	0.27	0.08
Ratio R	0.43	0.94	0.97	1.03

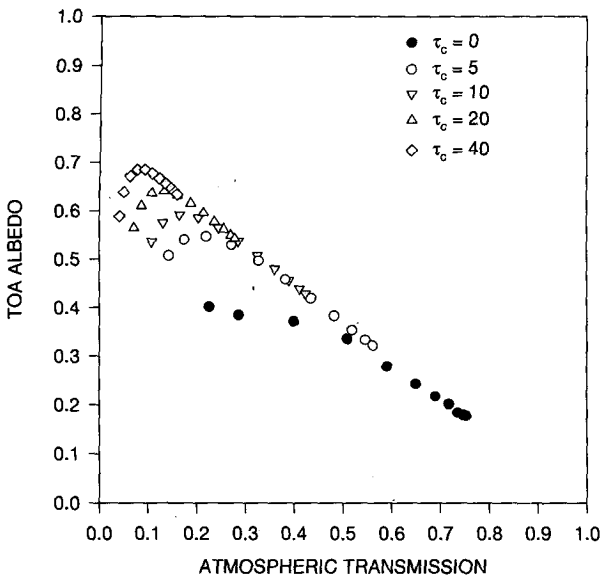

FIG. 4. Relationship between instantaneous TOA albedo and atmospheric transmittance. The same atmospheric, cloud, and surface conditions as in Fig. 1 are employed except that cloud optical thickness τ_c changes from 0 to 40.

for the corresponding instantaneous relationship. Furthermore, averaging over τ and cloud amount has little effect on the relationships.

Figure 5 presents the results of sensitivity tests for diurnal-mean relationships simulated for different months and latitudes. As expected, the relationships are more linear compared to the instantaneous cases. The slope is, however, extremely sensitive to surface type (which are distinguished primarily by albedo), moderately sensitive to cloud altitude, and weakly dependent on aerosol loading and cloud type. These results are understandable from the sensitivities of R to the same variables and the relationship between R and s given by (4). As a result, one should be cautious to conduct and interpret the linear regression between these two variables. Mixed use of data collected under different conditions, especially surface albedo, could lead to misleadingly low values of s as shown later.

4. Data

It follows from (1) that determination of R requires four quantities: $F^{\text{all}}_{\text{TOA}}$, $F^{\text{clr}}_{\text{TOA}}$, $F^{\text{clr}}_{\text{SFC}}$, and $F^{\text{all}}_{\text{SFC}}$. Similar to Ramanathan et al. (1995), the first three quantities were derived from ERBE satellite measurements. The $F^{\text{all}}_{\text{SFC}}$ terms were obtained by multiplying surface-based measurements of irradiance (or insolation) available from the Global Energy Balance Archive (GEBA) and the estimates of surface co-albedo ($1 - \alpha_s$) from ERBE. Determination of the slope as used in Cess et al. (1995) requires only all-sky surface irradiance to compute t_a and TOA all-sky net or reflected flux to derive α_p.

ERBE was a three-satellite program designed to monitor TOA radiative fluxes. ERBE measurements made with broadband scanning radiometers were available from 1985 to 1990. The data collected by these scanners have relatively high spatial resolution (about 50 km at nadir) but are subject to large uncertainties owing to insufficient angular sampling. Although the problem is alleviated by the ERBE angular dependence models that convert radiance into flux, the standard deviation (SD) error for an instantaneous ERBE shortwave (SW) pixel measurement resulting from inadequate angular correction is still as large as 38 W m^{-2}, more than six times the error associated with calibration (6 W m^{-2}) (Wielicki et al. 1995). These errors diminish quickly when the measurements are averaged, owing to error cancelation. For the monthly and regional mean ERBE product ($S - 4$), the total SD error for SW flux diminishes to 5 W m^{-2} (Wielicki et al. 1995). It should be pointed out, however, that this value is not a definite estimate of the uncertainty due to the lack of "ground truth" for the TOA flux (Barkstrom et al. 1989). At any rate, the monthly mean ERBE data are much more accurate than instantaneous data. In addition to all-sky TOA fluxes, ERBE also provides clear-sky TOA fluxes based on its scene identification algorithm. Although no meticulous analyses were done regarding the uncertainties in the clear-sky data, it is envisaged that the uncertainties are larger than for all-sky data for the following reasons. First, the ERBE scene identification scheme may misidentify cloudy scenes as clear simply on account of the definition of ERBE clear scenes, cloud amount less than 5%. Second, the presence of clouds reduces the number of clear-sky measurements and thus increases sampling error, which can be a serious problem for regions with persistent cloud coverage. When the ERBE clear-sky fluxes are used together with all-sky fluxes to determine CRF, an additional problem arises. In theory, CRF should be determined from a clear-sky measurement made under exactly the same condition as an all-sky measurement, which is unfortunately impossible in practice. Clear skies only occur when the weather condition is unfavorable to the formation of cloud, for example, less water vapor content. However, this simplification was shown to be a relatively minor problem for monthly mean SW CRF (Zhang et al. 1994; Barker 1995).

Surface irradiance measurements were made under the auspices of the worldwide radiation network operated by many countries around the world. After initial processing and quality screening, the data were reported to the World Radiation Data Center at St. Petersburg, Russia. Monthly mean values of surface irradiance and other components of surface energy budget for individual stations were further processed and archived as GEBA at the Swiss Federal Institute of Technology, where rigorous quality controls were implemented (Ohmura and Gilgen 1991). These site-spe-

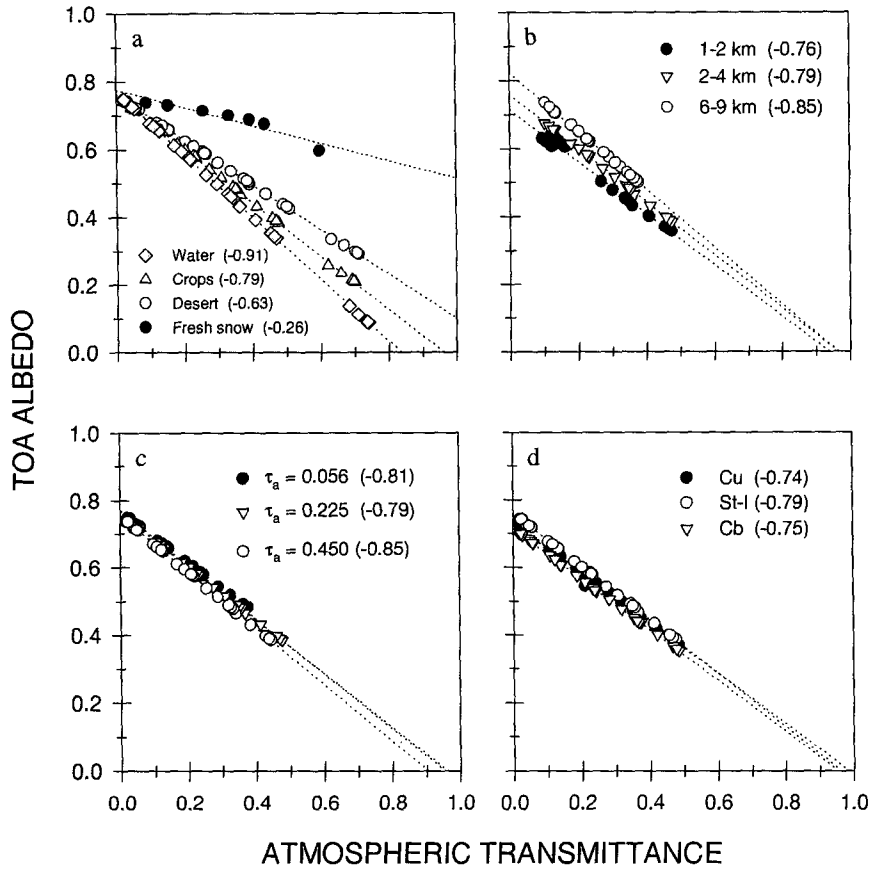

FIG. 5. Relationship between diurnal-mean TOA albedo and atmospheric transmittance for various surface, cloud, and atmospheric conditions: (a) four surface types, (b) three cloud heights, (c) three aerosol loadings, and (d) three cloud types. Unless stated otherwise, the conditions are the same as in Fig. 4. The slopes of the regression lines are in parentheses.

cific data were then averaged over cells of equal area 280 km × 280 km, a grid system employed in the International Satellite Cloud Climatology Project (ISCCP C1 grid cells), at the NASA Langley Research Center for validating the World Climate Research Project (WCRP) surface radiation budget (SRB) dataset (Whitlock et al. 1995). All GEBA data were stored in this dataset except those made over unusually polluted regions, mountains, and frequently foggy areas in order to improve spatial representativeness of the data. After numerous steps of screening, there remained approximately 100 cells with ground observations, the majority of which are located in the midlatitudes (Fig. 6a). While most of the cells contain only one station, cells in western Europe have up to ten stations. The total number of stations retained in the WCRP/SRB is less than 130. In comparison, the total number of stations equipped with pyranometers in the early 1990s is around 2000, which are distributed in 124 countries, 600 of which had over 10 years of observations (Ohmura and Gilgen 1993). Data volume reduction is also seen from the number of data months (Fig. 6b), which ranges from fewer than five at high latitudes to more than 40 in Germany. Nevertheless, the accuracy of irradiance measurements is limited by radiometric calibration of pyranometers. The accuracy of most pyranometers is estimated to be better than 15 W m^{-2} (Ohmura and Gilgen 1993). In addition to GEBA, the TOA all-sky and clear-sky ERBE data over the ISCCP C1 cells are also available from the WCRP/SRB.

Unfortunately, no monthly mean surface clear-sky net flux measurements are available from GEBA. They were thus obtained by means of remote sensing. Although clear-sky surface data were available from WCRP/SRB, these data were estimated from noncalibrated and narrowband radiances measured by operational satellites and thereby have potentially large uncertainties. As such, we decided to use the surface clear-sky net fluxes inferred from ERBE TOA data using the algorithm of Li et al. (1993a). The algorithm was developed on the basis of extensive radiative transfer modeling for a variety of atmospheric and surface conditions. It consists of a linear relationship between surface net flux and TOA reflected flux with the coef-

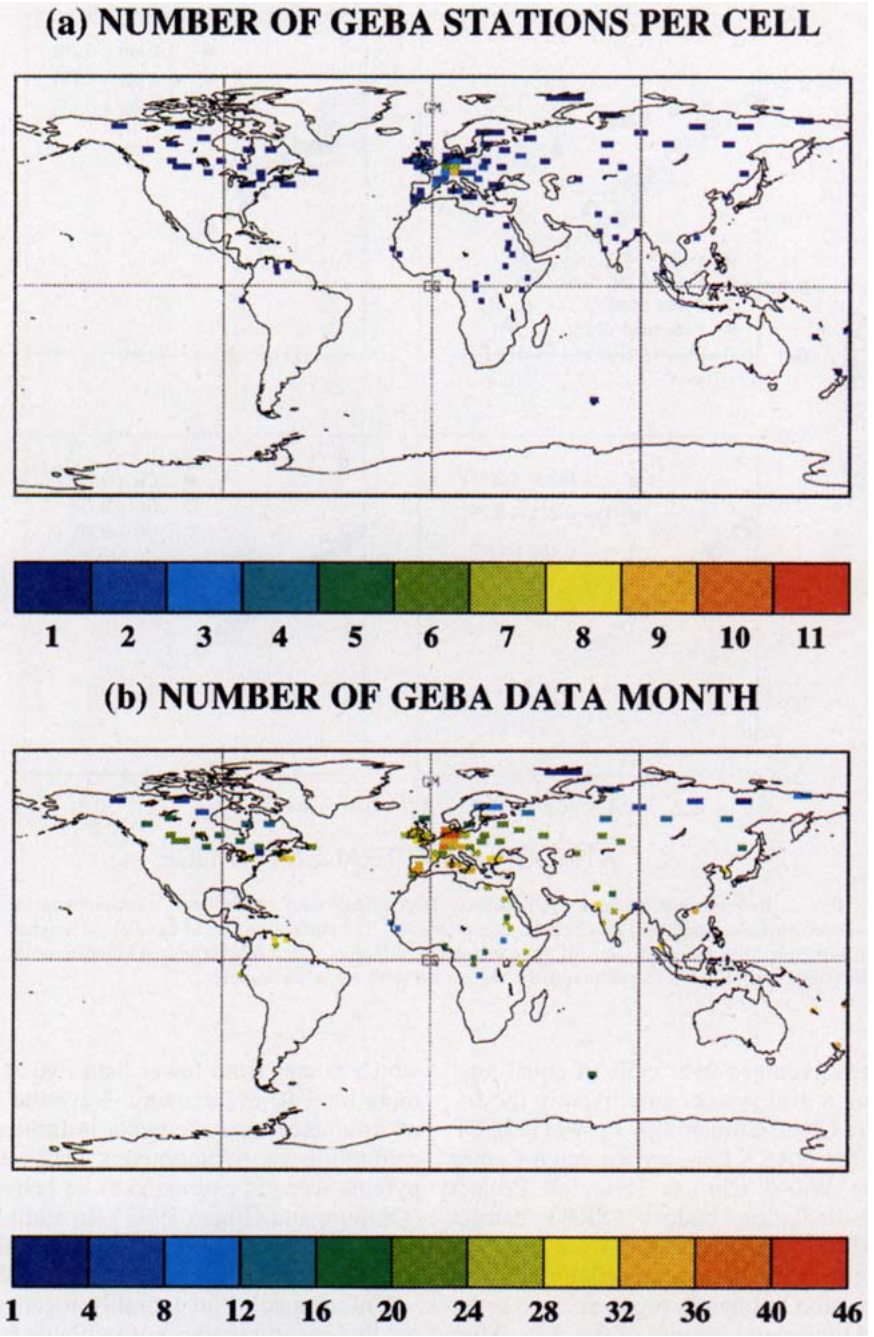

FIG. 6. Geographic distribution of ISCCP C1 cells (280 km)^2 containing GEBA surface radiation stations: (a) number of pyranometers per ISCCP C1 cell; (b) number of months with surface irradiance measurements between March 1985 and December 1988 inclusive.

ficients being functions of SZA and precipitable water. While the new version of the algorithm includes aerosol as an additional input parameter (Masuda et al. 1995), lack of aerosol data on global scale disables its utility for this study. Precipitable water data were obtained from the TOVS soundings contained in the WCRP/SRB. So far, validations of clear-sky flux estimates with surface observations have showed good agreements with almost no bias errors and moderate random errors (Li et al. 1993b; Ramanathan et al. 1995).

While surface albedo was observed at some radiation stations, the measurement merely represents a few tens of square meters. To match with other variables aver-

aged over a much larger area, all-sky surface albedos for the same ISCCP C1 grids were obtained from the WCRP/SRB dataset that were retrieved from ERBE TOA measurements using Staylor's algorithm (Darnell et al. 1992). The retrieval procedure had two steps. First, clear-sky surface albedo was derived from the clear-sky TOA ERBE data (Staylor et al. 1990). Second, corrections were applied to the retrieved clear-sky surface albedos to account for the effect of cloud cover using atmospheric transmittance inferred from TOA reflectance. Preliminary validations using surface albedo measurements made in the South Pole, central Greenland, and the Amazon rainforest showed that the estimates are accurate to within 8% of the surface-measured fraction values (Whitlock et al. 1995). Owing to meager surface albedo observations, the clear-sky component of surface albedos from Staylor et al. (1990) were also compared to the independent estimates by Li and Garand (1994) and Barker and Davies (1989). In general, the agreements are good. Nevertheless, this variable may be least reliable among the variables relevant to determination of R, owing to our poor knowledge and extreme shortage of ground-truth data.

When gridded surface data are used in conjunction with satellite data, an additional error arises from temporal and spatial differences between the two types of data. These errors are maximum for instantaneous observations and are reduced considerably when monthly mean data are considered. This is because instantaneous measurements are very sensitive to cloud variability. For monthly and regional mean data as employed in this study, temporal match-up error stems mainly from insufficient diurnal sampling by ERBE, whereas spatial match-up error is due to low density of pyranometers over a grid cell. On average, ERBE provides two daytime measurements. However, the problem is somewhat alleviated by the variable sampling time of the Earth Radiation Budget Satellite (ERBS) and the use of a temporal-averaging scheme (Brooks et al. 1986). The standard error associated with temporal sampling in ERBE monthly and regional mean data was estimated to be 2.6 W m^{-2} (Wielicki et al. 1995). This component of the matchup error is of both systematic and random nature since one of the ERBE aboard satellite (NOAA) provided measurements at the same local time, whereas ERBS collected data at varying local time. The matchup error arising from inadequate spatial sampling in the gridded GEBA data depends on the number of surface stations per cell. The dependence follows approximately $24.2N^{-1}$ W m^{-2}, where N is the number of stations per cell (Li et al. 1995b). Thus, as N changes from 1 to 10 (cf. Fig. 6a), matchup errors for individual months diminish from 24 to less than 3 W m^{-2}. This component of matchup error is, in general, of random nature unless the radiation station is situated in a region controlled by a local weather regime. As mentioned earlier, data from such locations have been kept from archiving in the WCRP/SRB.

All matched satellite and surface data were used except those for snow-covered land and frozen water. These data were discarded for two reasons. First, as shown in section 2, values of both R and s for bright surfaces are much different from those for other surfaces. Since this study aimed at investigating the impact of clouds on atmospheric absorption, the overwhelming influence of snow and/or ice should be eliminated. Second, ERBE scene identification over snow and ice surfaces is unreliable (Li and Leighton 1991), as are the resulting $\mathrm{CRF}_{\mathrm{TOA}}$ and the estimates of $F^{\mathrm{clr}}_{\mathrm{SFC}}$. The excluded pairs were identified as follows: if monthly mean clear-sky TOA albedo is less than 0.3, the cell is considered to be snow- or ice-free for that month. This simple criterion is based on variations of TOA clear-sky albedo with cosine of the SZA presented in Fig. 7. Despite significant dependencies on SZA, TOA clear-sky albedos exhibit two distinct clusters representing snow- and ice-free data and snow- and ice-covered data that are separated well by TOA albedo of 0.3. Use of this criterion may eliminate a few data points that appear to be open water for the cosine of SZA less than

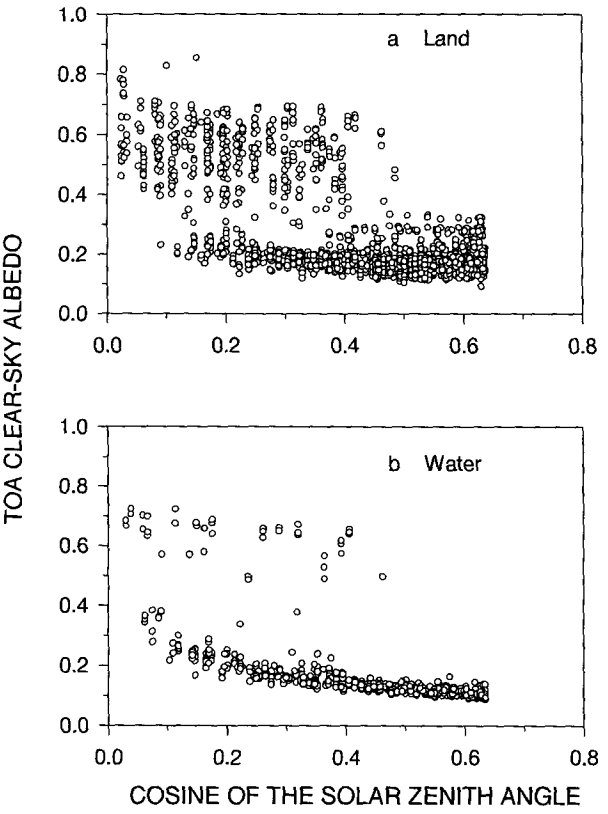

FIG. 7. Scatterplots of clear-sky monthly mean TOA albedo as a function of daytime, monthly mean cosine of the solar zenith angle over (a) land and (b) water.

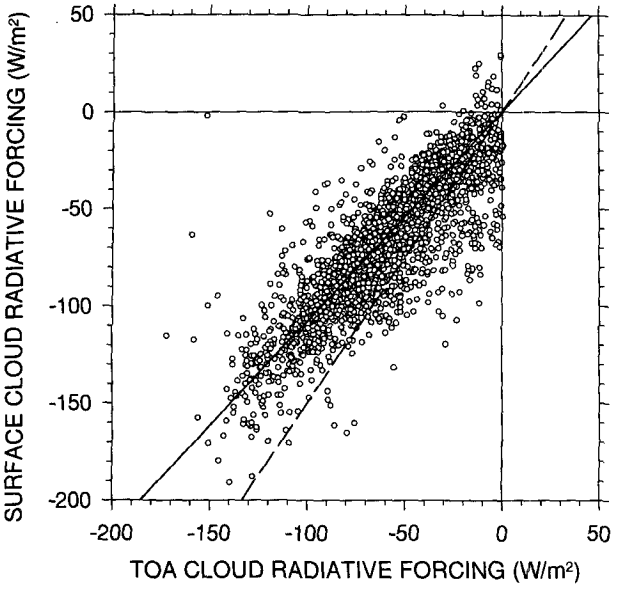

FIG. 8. Comparison between shortwave cloud radiative forcing at the TOA and at the surface. The solid line is obtained by least squares, linear regression of the points with intercept forced through the origin. The slope of 1.08 represents the overall ratio of surface to TOA cloud radiative forcing. For comparison, the dashed line representing $R = 1.5$ is added.

0.1 and snow-free land for the cosine of SZA larger than 0.5 (presumably deserts). The fraction of ill-classified months is, however, very small. After this screening, 2458 pairs of monthly mean data remain for analysis.

5. Analysis

a. Ratio

Figure 8 shows the relationship between TOA and surface CRF. A least squares linear regression led to a slope 0.93 and intercept −11.4. In theory, the intercept should go through the origin. The nonzero intercept stems from the finite number of samples and potential errors in the estimates of clear-sky surface net fluxes. If the intercept was set to zero, the slope became 1.08, which represents the overall ratio of surface to TOA cloud radiative forcing. The dashed line on Fig. 8 corresponds to $R = 1.5$. Clearly, the analysis presented here bears little resemblance to $R = 1.5$, even if statistical uncertainty is taken into account. At a confidence level 0.99, the overall value of R ranges from 1.05 to 1.11. As the outliers in Fig. 8, albeit a few, may have an overweening effect on the coefficients of the least square regression, the median-fitting method (Press et al. 1992), which minimizes absolute deviation instead of square difference, was conducted. The fitted intercept and slope turned out to be −5.2 and 1.0, respectively. When the intercept was forced to 0, the slope became 1.08 again. Therefore, we are confident, at least from the statistical point of view, that the overall value of R is definitely far less than 1.5 and is in good agreement with conventional radiative transfer models.

At first glance, it is surprising to note that there are 22 points in Fig. 8 (less than 1% of the total data) with positive CRF_{SFC}, meaning that surface net solar fluxes for all skies exceed those for clear skies. On a monthly and regional basis, this is unlikely to be true. Note, however, that these cases correspond to low CRF_{TOA} (generally less than 20 W m^{-2}), implying that there are few clouds present. Further investigations indicate they usually occur in subtropical high pressure regions, where the scarcity of clouds renders CRF_{SFC} close to zero. Due to uncertainties in both F^{all}_{SFC} and F^{clr}_{SFC} and their matchup errors, their difference, CRF_{SFC}, may be positive or negative. Noting that, on average, there are 1.5 stations per ISCCP C1 cell, a matchup error of approximately 16 W m^{-2} is expected. This is born out of Fig. 8, where for any given CRF_{TOA} the majority of points are within ±16 W m^{-2} of the regression line. Hence, as CRF_{TOA} becomes very small, it is expected that some values of CRF_{SFC} will be positive. By the same token, one would expect to find some points of positive CRF_{TOA} in view of the uncertainties in TOA fluxes as discussed earlier. Surprisingly, however, the data has a clear cut near $CRF_{TOA} = 0$. No positive values have been scrubbed out in this analysis. Therefore, ERBE scene identification must have implemented a constraint that excludes CRF_{TOA} at large positive values. Also, Fig. 8 shows that both CRF_{SFC} and CRF_{TOA} vary considerably with medians near −60 W m^{-2} and minima about −160 W m^{-2}.

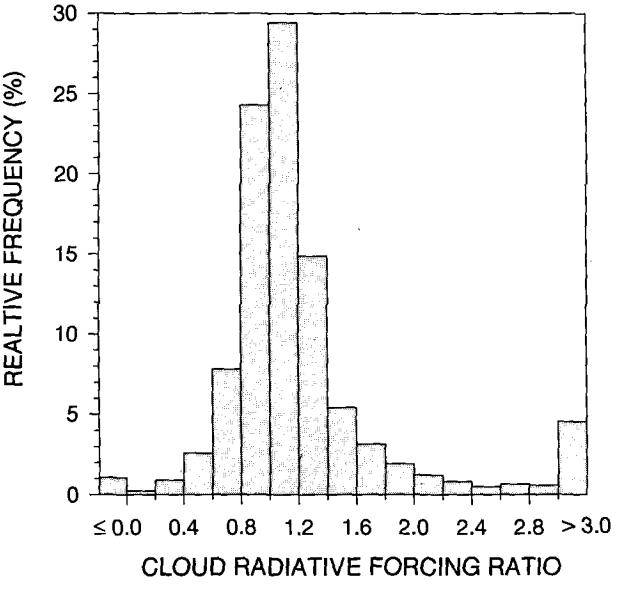

FIG. 9. Histogram of the relative occurrence frequency for all monthly values of R.

The variation of R is seen from the histogram of relative frequency for all monthly R presented in Fig. 9. It is interesting to note that the median of the histogram is the same as the slope of the regression line shown in Fig. 8. While 87% of R ranges from 0.6 to 2.0, the extreme values are −72 and 83. These extreme values of R are meaningless since they correspond to trace amounts of cloud with CRF_{TOA} near zero. As CRF_{TOA} approaches zero, R becomes increasingly sensitive to errors in CRF_{TOA}. Therefore, more credit should be given to R with large $|CRF_{TOA}|$. Figure 10 shows the observed and simulated variations of R with CRF_{TOA} for R between −5 and 10. The asymptotic number of observed R corresponding to very large $|CRF_{TOA}|$ is slightly above unity (1.0–1.1), which coincides well with those from GCMs and satellite-based TOA to surface transfer algorithms (e.g., Li et al. 1993a). The impact of potential errors in both CRF_{SFC} (ΔCRF_{SFC}) and CRF_{TOA} (ΔCRF_{TOA}) is delineated by the curves in Fig. 10 that envelop the simulated data points (not shown) by

$$R = \frac{CRF_{SFC}}{CRF_{TOA}} = \frac{CRF_{SFC} + \Delta CRF_{SFC}}{CRF_{TOA} + \Delta CRF_{TOA}}. \quad (5)$$

Assuming the true value of R is 1.05, that is, $CRF_{SFC} = 1.05\ CRF_{TOA}$, and $\Delta CRF_{SFC} = \Delta CRF_{TOA} = \Delta CRF$, simulated distributions of R versus CRF_{TOA} similar to the observed one were obtained by randomly changing CRF_{TOA} within the range of 0 to −200 W m^{-2} and ΔCRF within varying ranges given by $|\Delta CRF|$ in the plot. The percentages of the observed data points that fall within the envelop of $|\Delta CRF| \leq 5$, 10, 15, 20 W m^{-2} are 57%, 85%, 95%, and 98%, respectively. These numbers and the similarity between the observed and simulated distributions indicate that random errors in the input data may play a significant role in the diversity of observed values of R, especially for small magnitudes of CRF_{TOA}.

Of course, variation in R cannot be attributed entirely to the random uncertainty in input data. The ratio R is expected to vary with location and season due to variations in cloud, surface, atmosphere, and diurnal mean SZA. Figure 11 presents the regional values of R computed from the mean CRF_{SFC} and CRF_{TOA} averaged over the entire data period. In contrast to a featureless distribution that one would expect if the variation in R were caused entirely by random errors, Fig. 11 exhibits some pronounced patterns. The most striking one is that R has a strong zonal variation. In tropical regions, R is significantly larger than unity implying that cloudy atmospheres absorb substantially more than do clear skies. As stated later, however, the large R in the Tropics may be spuriously enhanced due to the effect of biomass burning. For midlatitudes (mostly the Northern Hemisphere), R is generally between 1.0 and 1.2, implying that cloudy-sky absorptance are slightly larger than those for clear skies. In polar regions, R is

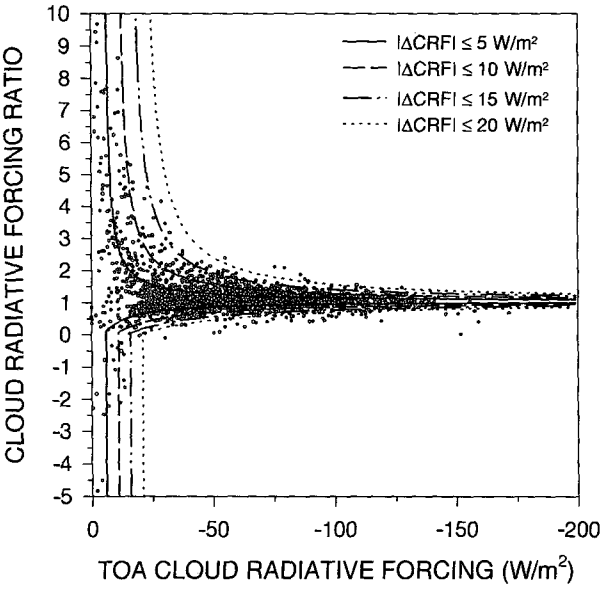

FIG. 10. Ratio R as a function of TOA shortwave cloud radiative forcing (open circles). Four curves depict the envelops encompassing simulated data points (not shown) for an assumed true value $R = 1.05$ and random uncertainty in CRF_{TOA} and CRF_{SFC} ranging from $-|\Delta CRF|$ to $|\Delta CRF|$.

less than 1, indicating that, when clouds are present, atmospheric absorption is reduced, compared to clear-sky absorption. It will be demonstrated later that the zonal variation of R is partially associated with changes in sun angle. The ratio R varies with longitude as well. For example, in the midlatitudes, R is greatest over Europe, intermediate over eastern Canada, and least in central Canada. This pattern corresponds approximately with anthropogenic aerosol loadings (Leaitch and Isaac 1991; Langner and Rodhe 1991). A close-up investigation of R over western Europe revealed that cells near Hamburg and the Rhine Valley have the largest values of R. These are known to be heavily polluted regions (Blanchet et al. 1986), and it is conceivable that absorption by low clouds is enhanced slightly by local absorbing aerosols (Chylek and Hallett 1992; Twomey 1972, 1977). Conversely, cells with the smallest values of R are near southern France and Ireland, which are relatively clean regions. Nevertheless, the possibility cannot be ruled out that these variations of R may be linked to regional variations of cloud and atmospheric constituents other than aerosol.

Both intra- and interannual variations of R are shown in Fig. 12, which includes 94 monthly values of R obtained from three cells in Germany to represent the midlatitude region. Each of these cells contains at least seven pyranometers, resulting in very small match-up errors between satellite and surface observations (less than 4 W m^{-2}). It is thus envisaged that the signal in the variation of R displayed in Fig. 12 outweighs the noise inherent in the determination of R. The dashed

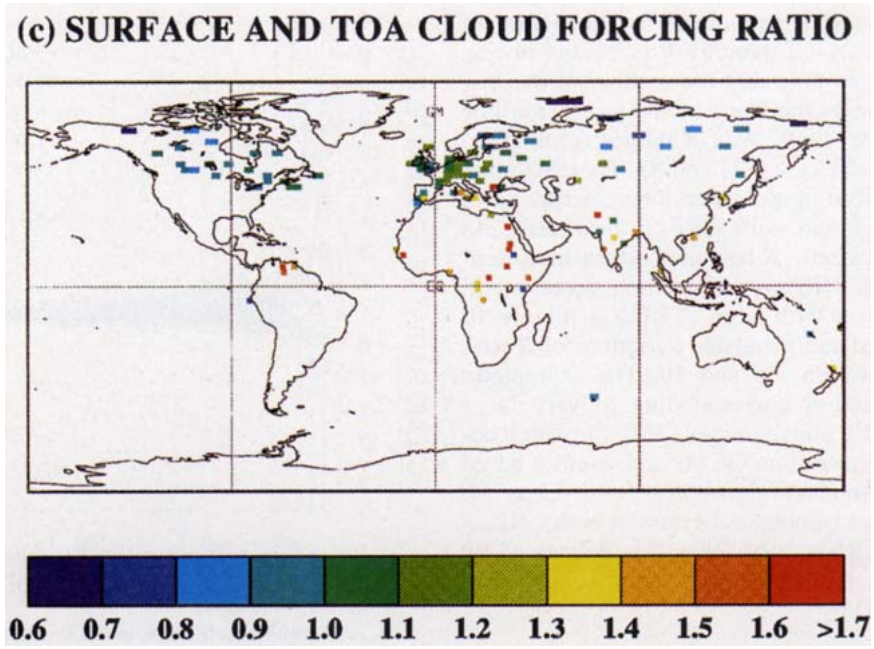

FIG. 11. Geographic distribution of R obtained from annual mean surface and TOA shortwave cloud radiative forcing using data from the entire data period (adapted from Li et al. 1995a; used with permission).

curve depicts the seasonal trend of R obtained from monthly means of CRF averaged over all data years. The smallest and largest values of R are less than 0.9 and larger than 1.15 occurring in winter and summer, respectively. The interannual variability of R is also striking: variations of 0.2–0.3 are not uncommon. In order to understand these variations, two modeled curves that encompass 85% of observed data are plotted. They were obtained from model simulations for two extreme conditions favoring high and low R. The thick curve represents a midlatitude summer atmosphere with CON-I aerosol of optical depth 0.45 and Cu cloud of optical depth 40 situated between 0 and 1 km. The thin curve corresponds to an aerosol-free, subarctic winter atmosphere with a St-I cloud of the same optical depth situated between 9 and 13 km. Land surface is used for both cases and the results are diurnal-mean values at 50°N. Comparing these curves with the dashed one suggests that the seasonal changes in R are governed partially by the seasonal variation in SZA. The remaining variation may be associated with changes in the atmosphere, surface, and clouds. Considering that the upper and lower bounds correspond to very extreme conditions that probably never exist on a monthly basis, values of R near and beyond them represent cases that are certainly inexplicable with conventional radiation models. If these values of R are trustworthy, they can serve as an unambiguous indication of cloud absorption anomaly. However, this is only observed for a small portion of the data under study.

A similar plot but for the Tropics is presented in Fig. 13. Despite a large plotting range in R (0–3), the data distribution is still all over the plotting domain. In contrast, a considerably narrower interval of the variation in R is found from model simulations with a tropical atmosphere over vegetated land at the equator. The thick and thin curves represent extreme values of R derived for the same aerosol and cloud conditions as in Fig. 12, except that cloud height of St-I cloud is 13–25 km instead of 9–13 km. Admittedly, 0–1 km for convective cloud is definitely not realistic in the Tropics where towering clouds generally reach much higher. Bear in mind, however, that an extreme value of R is being sought here. Owing to small seasonal changes in SZA, simulated R in the Tropics has little variation from month to month with fixed cloud conditions. Larger seasonal fluctuation in observed R is indicated by the dashed curve in Fig. 13. Despite the fact that the upper theoretical limit of R applies to cloud and aerosol conditions that are impossible to occur, many values of R still exceed this limit.

One should be aware, however, that the values of R determined in this region are less reliable than those in midlatitudes for several reasons. First, GEBA data suffer larger sampling errors due to lower station density and more frequent presence of convective types of clouds. Second, R is more vulnerable to errors in the input data, owing to lower absolute values of CRF_{TOA}, as is seen clearly from the comparison between the histograms of CRF_{TOA} in the Tropics and in the midlatitudes (Fig. 14). Third, aerosol loading is larger and

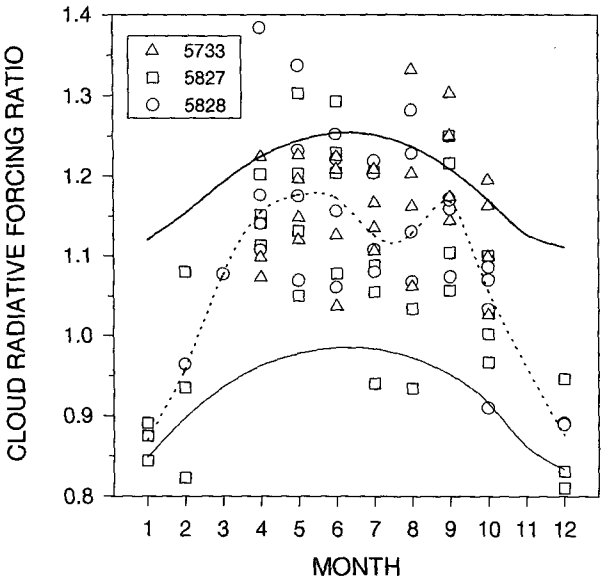

FIG. 12. Monthly R for three German cells containing at least seven pyranometers per cell. The numbers on the plot are the ISCCP C1 cell numbers that correspond to latitude and longitude: 5827 (51°15′N, 10°E), 5828 (51°15′N, 10°E), and 5733 (48°45′N, 9°28′E). The thick and thin curves are computed with the plane-parallel model for conditions favoring extremely high and low values of R. The dashed curve delineates seasonal variation of R computed from the mean values of cloud radiative forcing at the surface and TOA averaged over all available years and sites for the same months (adapted from Li et al. 1995a; used with permission).

more variable in the regions surrounding many tropical GEBA stations. The effect of aerosol (absorbing) on R is twofold: truly raising R due to enhanced absorption within a cloud and falsely increasing R as a result of the overestimation of surface clear-sky flux by the algorithm of Li et al. (1993a). The algorithm is particularly prone to errors for strong absorbing aerosols (Masuda et al. 1995), such as those produced from biomass burning. It is well known that fires are popular over extended areas of the tropical landmass, especially in Africa, South America, and Southeast Asia where majority of the tropical GEBA stations are located (Crutzen and Andreae 1990; Cahoon et al. 1992). These burns produce large amounts of graphic (black) carbon, a strong absorber of solar radiation in the solar spectrum (Chylek et al. 1984; Chylek and Hallett 1992). The single-scattering albedo and optical thickness of the biomass burning aerosol vary considerably with season and location (Lenoble 1991; Kaufman et al. 1992, 1994). This may explain qualitatively why R is larger and more variable in the Tropics than in the midlatitudes. Although lack of aerosol data prevents us from confirming this quantitatively, the following two findings are at least in support of the argument. First, the maximum in the seasonal trend of R (dashed curve in Fig. 13) happens to occur during the dry season (January–April) in many tropical regions (GPCC 1992). Low precipitation rate does not only facilitate more fires (Cahoon et al. 1992), which renders high density of black carbon (Cachier et al. 1989), but it also amplifies its impact on atmospheric absorption owing to the prolonged residence of aerosols in the atmosphere. Second, all satellite-based estimates of all-sky surface insolation are too high in the Tropics but agree much better with surface observations in the midlatitudes (a manuscript in preparation).

b. Slope

As mentioned earlier, regression analyses were also conducted between the monthly mean planetary albedo and atmospheric transmittance (Cess et al. 1995). Although this approach avoids the uncertainties associated with the inference of surface albedo and clear-sky surface net flux, it has an inherent limitation: not allowing determination of the slope for each site and month. When multiple data points are used to perform a regression, it should be cautious not to mix the effects of such factors as surface condition into the slope. The following discussion demonstrates how this effect could lead to misleading values of s.

Figure 15a shows the relationship for all GEBA measurements. The distribution pattern bears a close resemblance to the model results presented in Fig. 5, owing to the existence of varying surface types. A linear least squares regression leads to $s = -0.53$, with a correlation coefficient of just 0.26. To lessen the impact of mixed surface types on s, data points were first clas-

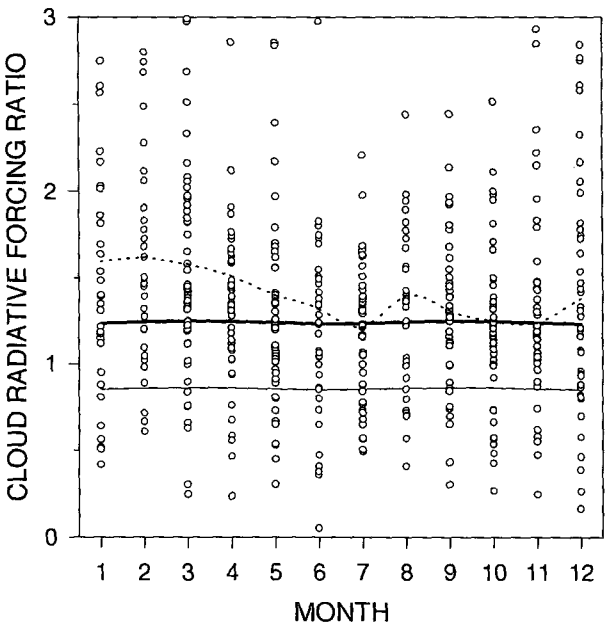

FIG. 13. Similar to Fig. 12 but for all the tropical data. For clarity, cell numbers are not distinguished. Data outside the plotting domain are not shown.

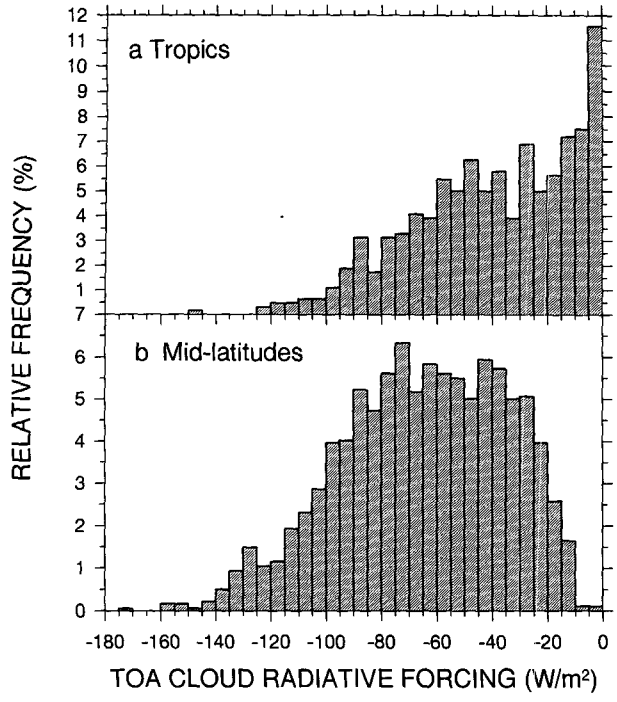

FIG. 14. Histograms of the relative frequency in TOA cloud radiative forcing in the (a) Tropics and (b) midlatitudes.

sified into either land or water categories based on surface geographic information provided by WCRP/SRB. Subsequent classification as either snow-free or snow-covered land, and open and frozen water was done by employing monthly mean clear-sky TOA albedo from ERBE. After separation, the linear relationships between α_p and t_a emerge clearly for both snow-free land (Fig. 15b) and open water (Fig. 15c). The relationships for snow-covered land and frozen water are still poor, presumably due to variations in coverage and age of snow and ice. Therefore, only regression results for snow-free land and open water are given in Figs. 15b and 15c. For open water, $s \approx -0.84$, to which the model results presented in Fig. 5a agrees reasonably well. The linearity of the relationship for water is better than for land because α_s for water is more uniform than for land as seen in Fig. 7. The range of α_p^{clr} for snow-free land delineated in Fig. 7 is testimonial to the fact that surface type is diverse, ranging from dense vegetation to bare sand. Points in Fig. 7 with α_p^{clr} near 0.3 for cosine of SZA larger than 0.5 correspond presumably to snow-free desert. It should be separated from vegetated land since their slopes are very different. Furthermore, the values of s shown in Fig. 15 are subject to large uncertainties associated with large match-up errors.

Figure 16 shows the same comparison as Fig. 15 but for cells containing multiple surface pyranometers. The total number of data points diminishes from 2983 to 888, but the average density of stations increases from 1.5 to 3.1 and thus reduces matchup error by a factor of 2. Besides, the distribution of land points shifts toward central western Europe where surface cover is fairly uniform. As a result, the linearity of the relationship improve for snow-free land. The correlation coefficient increases from 0.65 to 0.83 and the slope decreases from −0.6 to −0.67. Although bright desert cells are not involved in Fig. 16, the diversity of non-desert land remains high. A variation of 10% in α_p^{clr} found at fixed SZAs (c.f. Fig. 7) suggests that surface types represented in Fig. 16 are still too variable to provide meaningful estimates of s. Therefore, only the data from three German cells were examined next. These cells have very similar surface conditions: for common values of SZA, differences in α_p^{clr} are generally less than 3%. Figure 17 shows an excellent linear relationship between α_p and t_a, with a correlation co-

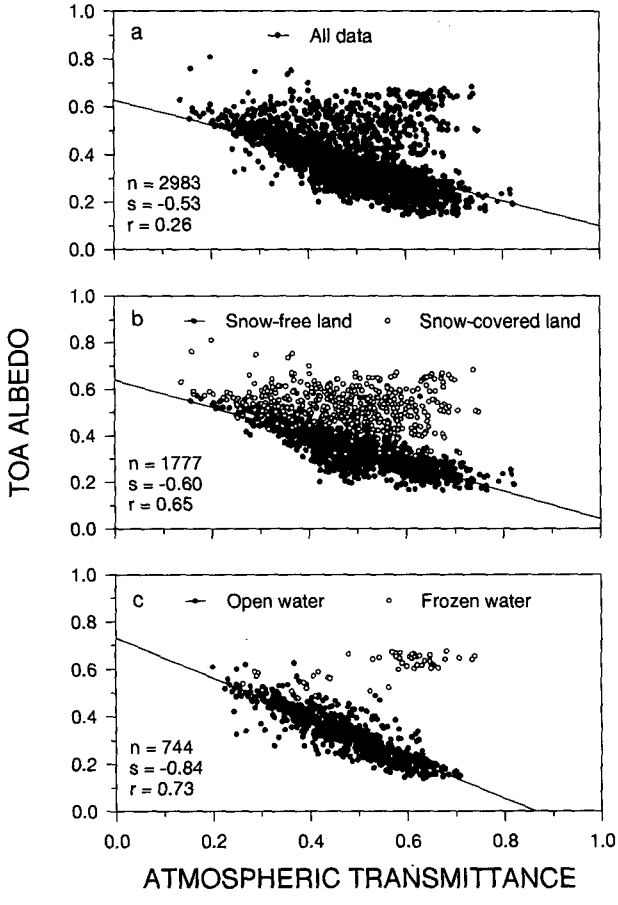

FIG. 15. Scatterplots of monthly mean TOA albedo measured by ERBE verses monthly mean atmospheric transmittance determined from surface measured insolation for (a) all data; (b) land only; and (c) water only. Linear regression analyses are made using all the data in (a), snow-free data in (b) and open-water data in (c). Parameters n, s, and r are the number of samples, slope, and correlation coefficient of the regressions, respectively.

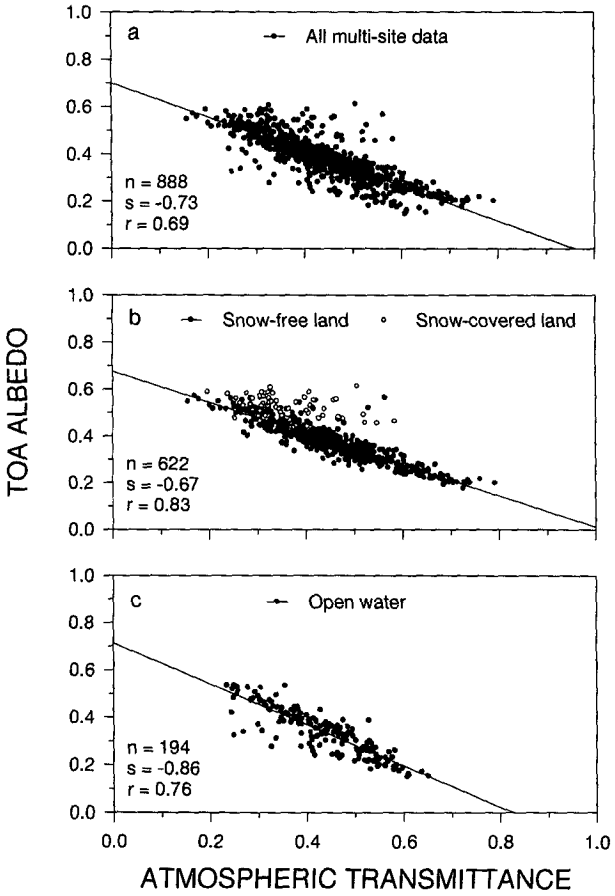

FIG. 16. Same as Fig. 15 except for cells with multiple pyranometers.

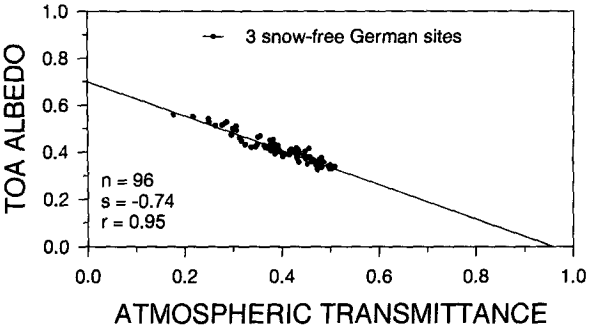

FIG. 17. Same as Fig. 15 except for three cells located in Germany, each of which contain at least seven pyranometers. The locations of these cells are indicated in the figure caption of Fig. 12 (adapted from Li et al. 1995a; used with permission).

efficient of 0.95. The value of s decreases to -0.74. The mean albedo for the three cells was estimated to be 0.150 using Staylor's algorithm and 0.153 using the algorithm of Li and Garand (1994). From (4), R was determined to be 1.14, which is very close to the value of R derived as the ratio of cloud radiative forcing.

Regression analyses were also made for individual ISCCP C1 cells containing at least three surface stations and more than two years of snow-free data. Eleven cells located throughout western Europe satisfy these requirements. Table 3 provides geographical information of these cells, numbers of stations and data months, correlation coefficients, and slopes of the linear regressions. Although data volume is not very large for each cell, high correlation coefficients, due to uniform surface conditions, bolster confidence in the results. Values of s ranged from -0.67 to -0.87 with a mean of -0.77.

So far we have followed the exactly same method as used by Cess et al. (1995) in order to show the differences caused by using different datasets. It is noted, however, that there is a potential problem regarding the selection of independent (X) and dependent (Y) variables. The standard linear regression assumes that X is measured with perfect accuracy, and thus regression coefficients are sought to minimize the sum of the squares of the Y residuals. If the reverse is true, one should treat Y as an independent variable and X as a dependent variable. The regression lines determined in two different ways will not be the same unless X and Y are perfectly correlated. The slopes differ by a factor of r^{-2}, where r is the correlation coefficient. For example, if the independent and dependent variables are exchanged in the regression of German data, the slope becomes $0.74/0.90 = -0.82$. Likewise, Arking et al. (1995) obtained a slope -0.72 instead of -0.59 using the same data appearing in Fig. 2a of Cess et al. (1995). When both variables are subject to uncertainties, which is true in many cases, the "best" least squares regression line should be obtained by minimizing the sum of squares of the perpendicular distance between data

TABLE 3. Slopes s and correlation coefficients r of the linear regressions between planetary albedo and atmospheric transmittance for 11 cells containing at least three GEBA radiation stations.

Cell	Latitude	Longitude	Stations*	Months**	s	r
5527	43.75°N	1.73°E	3.0	29	−0.87	0.94
5631	46.25°N	1.80°E	3.0	26	−0.83	0.97
5732	48.75°N	9.47°E	4.0	26	−0.76	0.93
5733	48.75°N	9.47°E	9.6	27	−0.67	0.90
5734	48.75°N	13.26°E	3.0	24	−0.76	0.89
5827	51.25°N	2.00°E	6.2	35	−0.72	0.95
5828	51.25°N	10.00°E	7.0	32	−0.77	0.95
5915	51.25°N	2.00°W	3.7	27	−0.73	0.89
5917	53.75°N	6.35°E	3.0	34	−0.79	0.92
5918	53.75°N	10.59°E	3.6	42	−0.69	0.89
5999	53.75°N	6.35°W	3.0	26	−0.84	0.87

* Mean number of radiation stations in a cell for all the months in which there are more than three stations. Note that the number of stations may vary from month to month.

** Only snow-free months are counted as determined by the clear-sky TOA albedo.

points and the straight line to be established. Yet each data point should be weighted properly according to its uncertainty. Depending on the weights, the "best" slope is not necessarily bounded by the values from the regressions of X on Y and Y on X, (York 1966). As a test, we applied this technique (Press et al. 1992) to the German data. The standard errors of the two variables were discussed in the data section. The new slope turns out to be -0.73, which differs very slightly from the original regression, with a standard uncertainty of 0.03.

6. Summary

The long-standing debate over the cloud absorption anomaly was reheated recently following some studies suggesting that the anomaly is a rather universal phenomenon with a much larger magnitude than what has been thought before. These studies inferred cloud absorption from the ratio R of cloud radiative forcing at the surface and at the top of the atmosphere and from the slope s of the linear regression between TOA albedo and atmospheric transmittance. This study examines the two parameters by means of both radiative transfer modeling and the use of global spaceborne and ground-based observations over a period up to 5 years.

The ratio R is not a direct measure of cloud absorption but may serve as an indicator of the impact of clouds on absorption of solar radiation by the entire atmospheric column relative to a clear atmosphere. The sensitivity of R to various parameters were determined using a plane-parallel radiative transfer model based on the doubling–adding method and conventional cloud optical properties. The ratio R is most sensitive to cloud height and solar zenith angle and moderately dependent on cloud microphysics, water vapor and aerosol content, and surface type except for snow and/or ice. Clouds may substantially increase atmospheric absorption if situated near the surface due to increased photon pathlengths through water vapor and aerosol. Nevertheless, the model rarely produces R larger than 1.25. Therefore, observations of R larger than 1.25 may prove the existence of a cloud absorption anomaly. On the other hand, however, R less than 1.25 does not necessarily disprove the existence of a cloud absorption anomaly. Therefore, R may not be valid for addressing cloud absorption anomaly if its magnitude is not as large as reported in recent studies. The slope s can be related to R with the knowledge of surface albedo when the relationship between TOA albedo and atmospheric transmittance is linear and surface albedo does not depend on cloud condition. Sensitivity tests showed that s is very sensitive to surface albedo, moderately sensitive to cloud and atmospheric conditions, and insensitive to solar zenith angle unless it is very large.

Monthly mean values of R were derived from TOA satellite measurements and surface pyranometer observations made around the globe. TOA shortwave CRF was obtained solely from ERBE, which provided both clear- and all-sky TOA fluxes. Surface CRF was based on all-sky ground-based observations of insolation and satellite-based estimates of clear-sky surface net solar radiation and all-sky surface albedo. Quality-controlled surface irradiances were made available from GEBA. The overall value of R obtained from both the regression between individual values of TOA and surface CRF and from the means of surface and TOA CRF is about 1.1. This is in good agreement with model calculations. Ratio R does, however, exhibit significant changes with location and season. In general, R is less than, approximately equal to, and greater than unity over the polar, midlatitude, and tropical regions, respectively. This implies that polar and tropical clouds have opposing effects on total atmospheric absorption, while midlatitude clouds have relatively little impact on absorption. It should be pointed out, however, that the large values of R for the tropical regions are less reliable than the moderate values for midlatitude areas. This is because of few surface observations, weak cloud radiative forcing and frequent biomass burning near the GEBA tropical sites. Regression analyses between TOA albedo and atmospheric transmittance were conducted for various data categories. The most reliable results were obtained when surface albedo varies little. In these cases, the values of R derived from s and surface albedo are approximately equal to those obtained directly from cloud radiative forcing. In addition to the standard regression method, some special regression methods such as median fitting and fitting with errors in both dependent and independent variables were employed, which did not distort the finding of this study. Therefore, we conclude that cloud-absorption anomaly, if it exists, is neither as common nor as large, as indicated from some recent studies.

Acknowledgments. We are grateful to the anonymous reviewers who offered many constructive and careful comments leading to a substantially improved version of the manuscript. The authors are particularly indebted to Dr. H. Barker for numerous discussions. The study also benefits from discussions with Drs. A. Arking, R. D. Cess, T. P. Charlock, M.-D. Chou, W. Rossow, W. Wiscombe, and M.-H. Zhang, to name a few. Dr. J. Chen provided a CCRS internal review of the original manuscript.

REFERENCES

Arking, A., M. D. Chou, and W. L. Ridgway, 1995: On estimating the effects of clouds on atmospheric absorption based on flux observations above and below cloud level. *Geophys. Res. Let.*, in press.

Barker, H. W., 1995: Methodological dependencies of cloud radiative forcing for the Canadian Climate Centre—Second generation general circulation model. *J. Geophy. Res.*, **100,** 1017–1025.

——, and J. Davies, 1989: Surface albedo estimates from Nimbus-7 ERB data and a two-stream approximation of the radiative transfer equation. *J. Climate,* **2,** 409–418.

——, and Z. Li, 1995: Improved simulation of clear-sky shortwave radiative transfer in the CCC-GCM. *J. Climate,* **8,** 2213–2223.

Barkstrom, B. R., E. F. Harrison, G. L. Smith, R. Green, J. Kibler, R. D. Cess, and the ERBE Science Team, 1989: Earth Radiation Budget Experiment (ERBE) archival and April 1985 results. *Bull. Amer. Meteor. Soc.,* **70,** 1254–1262.

Blanchet, J.-P., J. Heintzenberg, and P. Winkler, 1986: Radiative heating during an intense pollution episode in Hamburg. *Beitr. Phys. Atmos.,* **54,** 143–158.

Braslau, N., and J. V. Dave, 1973: Effect of aerosols on the transfer of solar energy through realistic model atmosphere. Part II: Non-absorbing aerosols. *J. Appl. Meteor.,* **12,** 601–615.

Brooks, D. R., E. F. Harrison, P. Minnis, and J. T. Suttles, 1986: Development of algorithms for understanding the temporal and spatial variability of the earth's radiation balance. *Rev. Geophys.,* **24,** 422–438.

Cachier, H., M.-P. Bremond, and P. Buat-Menard, 1989: Carbonaceous aerosols from different tropical biomass burning sources. *Nature,* **340,** 371–373.

Cahoon, D. R., Jr., B. J. Stocks, J. S. Levine, W. R. Cofer III, and K. P. O'Neill, 1992: Seasonal distribution of African savanna fires. *Nature,* **359,** 812–815.

Cess, R. D., and Coauthors, 1993: Uncertainties in carbon dioxide radiative forcing in atmospheric general circulation models. *Science,* **262,** 1252–1255.

——, and Coauthors, 1995: Absorption of solar radiation by clouds: Observations versus models. *Science,* **267,** 496–499.

Chou, M.-D., A. Arking, and W. L. Ridgway, 1995: The effect of clouds on atmospheric heating. *Geophys. Res. Lett.,* **22,** 1885–1888.

Chylek, P., and J. Hallett, 1992: Enhanced absorption of solar radiation by cloud droplets containing soot particles on their surface. *Quart. J. Roy. Meteor. Soc.,* **118,** 167–172.

——, V. Ramaswamy, and R. J. Cheng, 1984: Effect of graphitic carbon on the albedo of clouds. *J. Atmos. Sci.,* **41,** 3076–3084.

Crutzen, P. J., and O. M. Andreae, 1990: Biomass burning in the Tropics: Impact on atmospheric chemistry and biogeochemical cycles. *Science,* **250,** 1669–1678.

Darnell, W. L., W. F. Staylor, S. K. Gupta, N. A. Ritchey, and A. C. Wilber, 1992: Seasonal variation of surface radiation budget derived from International Satellite Cloud Climatology Project C1 data. *J. Geophys. Res.,* **97,** 15 741–15 760.

Foot, J. S., 1988: Some observations of the optical properties of clouds. Part I: Stratocumulus. *Quart. J. Roy. Meteor. Soc.,* **114,** 129–144.

Fouquart, Y., B. Bonnel, and V. Ramaswamy, 1991: Intercomparing shortwave radiation codes for climate studies. *J. Geophys. Res.,* **96,** 8955–8968.

Fritz, S., 1951: Solar radiant energy. *Compendium of Meteorology,* T. F. Malone, Ed., Wiley and Sons, 14–29.

Garratt, J. R., 1994: Incoming shortwave fluxes at the surface—A comparison of GCM results with observations. *J. Climate,* **7,** 72–80.

GPCC (Global Precipitation Climatology Centre), 1992: *Monthly Precipitation Estimates Based on Gauge Measurements on Continents for the Year 1987 (Preliminary Results and Future Requirements).* Deutscher Wetterdienst, 20 pp.

Harrison, E. F., P. Minnis, B. R. Barkstrom, V. Ramanathan, R. D. Cess, and G. G. Gibson, 1990: Seasonal variation of cloud radiative forcing derived from the earth radiation budget experiment. *J. Geophys. Res.,* **95,** 18 687–18 703.

Hayasaka, T., N. Kikuchi, and M. Tanaka, 1995: Absorption of solar radiation by stratocumulus clouds: Aircraft measurements and theoretical calculations. *J. Appl. Meteor.,* **34,** 1047–1055.

Herman, G. F., and J. A. Curry, 1984: Observational and theoretical studies of solar radiation in Arctic stratus clouds. *J. Climate Appl. Meteor.,* **23,** 5–24.

Hignett, P., 1987: A study of the short-wave radiative properties of marine stratus: Aircraft measurements and model comparisons. *Quart. J. Roy. Meteor. Soc.,* **113,** 1011–1024.

Iqbal, M., 1983: *An Introduction to Solar Radiation.* Academic Press, 390 pp.

Kaufman, Y. J., A. Setzer, D. Ward, D. Tanre, B. N. Holben, P. Menzel, M. C. Pereira, and R. Rasmussen, 1992: Biomass burning airborne and spaceborne experiment in the Amazon (BASE-A). *J. Geophy. Res.,* **97,** 14 581–14 599.

——, D. Tanre, and D. E. Ward, 1994: Remote sensing of biomass burning in the Amazon. *Remote Sens. Rev.,* **10,** 51–90.

King, M. D., 1993: Radiative properties of clouds. *Aerosol-Cloud-Climate Interactions,* P. V. Hobbs, Ed., Academic Press, 123–149.

——, L. F. Radke, and P. V. Hobbs, 1990: Determination of the spectral absorption of solar radiation by marine stratocumulus clouds from air-borne measurements within clouds. *J. Atmos. Sci.,* **47,** 894–907.

Langner, J., and H. Rodhe, 1991: A global three-dimensional model of the tropospheric surface cycle. *J. Atmos. Chem.,* **13,** 225–263.

Leaitch, W. R., and G. A. Isaac, 1991: Tropospheric aerosol size distributions from 1982 to 1988 over eastern North America. *Atmos. Env.,* **25A,** 601–619.

Lenoble, J., 1991: The particulate matter from biomass burning: A tutorial and critical review of its radiative impact. *Global Biomass Burning: Atmospheric, Climatic, and Biospheric Implications,* J. S. Levine, Ed., MIT Press, 381–386.

Li, Z., and H. G. Leighton, 1991: Scene identification and its effect on cloud radiative forcing in the Arctic. *J. Geophy. Res.,* **96,** 9175–9188.

——, and H. W. Barker, 1994: Solar energy disposition: Intercomparison between satellite estimation, GCM simulation, and surface observation. Cloud-radiation interaction and their parameterization in climate models, WCRP-86, WMO/TD-No. 648, 110–113.

——, and L. Garand, 1994: Estimation of surface albedo from space: A parameterization for global application. *J. Geophys. Res.,* **99,** 8335–8350.

——, H. G. Leighton, K. Masuda, and T. Takashima, 1993a: Estimation of SW flux absorbed at the surface from TOA reflected flux. *J. Climate,* **6,** 317–330.

——, ——, and R. D. Cess, 1993b: Surface net solar radiation estimated from satellite measurements: Comparisons with tower observations. *J. Climate,* **6,** 1764–1772.

——, H. W. Barker, and L. Moreau, 1995a: The variable effect of clouds on atmospheric absorption of solar radiation. *Nature,* **376,** 486–490.

——, C. H. Whitlock, and T. P. Charlock, 1995b: Assessment of the global monthly mean surface insolation estimated from satellite measurements using global energy balance archive data. *J. Climate,* **8,** 315–328.

Masuda, K., H. G. Leighton, and Z. Li, 1995: A new parameterization for the determination of solar flux absorbed at the surface from satellite measurements. *J. Climate,* **8,** 1615–1629.

McClatchey, R. A., R. W. Fenn, J. E. A. Selby, F. E. Volz, and J. S. Garing, 1972: Optical properties of the atmosphere. Environ. Res. Paper 411, 110 pp.

Ohmura, A., and H. Gilgen, 1991: *Global Energy Balance Archive (GEBA),* World Climate Program—Water Project A7, Report 2: The GEBA Database, Interactive Application, Retrieving Data. Verlag der Fachvereine, 60 pp.

——, and ——, 1993: Reevaluation of the global energy balance. *Geophys. Monogr.,* No. 75, IUGG, 93–110.

Pilewski, P., and F. Valero, 1995: Direct observations of excess solar absorption by clouds. *Science,* **257,** 1626–1629.

Press, W. H., S. A. Teukolsky, W. T. Vetterling, and B. P. Flannery, 1992: *Numerical Recipes in C.* Cambridge University Press, 994 pp.

Ramanathan, V., R. D. Cess, E. F. Harrison, P. Minnis, B. R. Barkstrom, E. Ahmad, and D. Hartmann, 1989: Cloud-radiative forcing and climate: Results from the Earth Radiation Budget Experiment. *Science,* **243,** 57–63.

——, B. Subasilar, G. J. Zhang, W. Conant, R. D. Cess, J. T. Kiehl, H. Grassl, and L. Shi, 1995: Warm pool heat budget and shortwave cloud forcing: A missing physics. *Science,* **267,** 499–503.

Rawlins, F., 1989: Aircraft measurements of the solar absorption by broken cloud fields: A case study. *Quart. J. Roy. Meteor. Soc.,* **115,** 365–382.

Reynolds, D. W., T. H. Vonder Harr, and S. K. Cox, 1975: The effect of solar radiation absorbtion in the tropical atmosphere. *J. Appl. Meteor.,* **14,** 433–444.

Robinson, G. D., 1958: Some observations from aircraft of surface albedo and the albedo and absorption of cloud. *Arch. Meteor. Geophys. Bioklimatol.,* **B9,** 28–41.

Rossow, W. B., and Y.-C. Zhang, 1995: Calculation of surface and top of atmosphere radiative fluxes from physical quantities based on ISCCP data sets, 2. Validation and first results. *J. Geophy. Res.,* **100,** 1167–1197.

Slingo, A., S. Nicholls, and J. Schmetz, 1982: Aircraft observations of marine stratocumulus during JASIN. *Quart. J. Roy. Meteor. Soc.,* **108,** 833–856.

Staylor, W. F., and A. C. Wilber, 1990: Global surface albedos estimated from ERBE data. *Proc. Seventh Conf. on Atmospheric Radiation,* San Francisco, CA, Amer. Meteor. Soc., 231–236.

Stephens, G. L., 1978: Radiation profiles in extended water clouds. Part I: Theory. *J. Atmos. Sci.,* **35,** 2111–2122.

——, 1995: Brightening the dark cloud paradox. *Science,* in press.

——, and C. M. R. Platt, 1987: Aircraft observations of the radiative microphysical properties of stratocumulus and cumulus cloud fields. *J. Climate Appl. Meteor.,* **26,** 1243–1269.

——, and S.-C. Tsay, 1990: On the cloud absorption anomaly. *Quart. J. Roy. Meteor. Soc.,* **116,** 671–704.

Twomey, S., 1972: The effect of cloud scattering on the absorption of solar radiation by atmospheric dust. *J. Atmos. Sci.,* **29,** 1156–1159.

——, 1977: The influence of pollution on the shortwave albedo of clouds. *J. Atmos. Sci.,* **34,** 1149–1152.

WCP-112, 1986: A preliminary cloudless standard atmosphere for radiation computation. World Climate Research Programme, WMO/TD-No. 24, 53 pp.

Whitlock, C. H., T. P. Charlock, W. F. Staylor, R. T. Pinker, I. Laszlo, A. Ohmura, H. Gilgen, T. Konzelman, R. C. DiPasquale, C. D. Moats, S. R. LeCroy, and N. A. Ritchey, 1995: First global WCRP shortwave surface radiation budget dataset. *Bull. Amer. Meteor. Soc.,* **76,** 905–922.

Wielicki, B. A., R. D. Cess, M. D. King, D. A. Randall, and E. F. Harrison, 1995: Mission to planet Earth: Role of clouds and radiation in climate. *Bull. Amer. Meteor. Soc.,* **76,** 2125–2153.

Wild, M., A. Ohmura, H. Gilgen, and E. Roeckner, 1995: Validation of general circulation model radiative fluxes using surface observations. *J. Climate,* **8,** 1309–1324.

Wiscombe, W. J., 1995: Atmospheric physics: An absorbing mystery. *Nature,* **376,** 466–467.

——, R. M. Welch, and W. D. Hall, 1984: The effects of very large drops on cloud absorption. Part I: Parcel models. *J. Atmos. Sci.,* **41,** 1336–1355.

York, D., 1966: Least-squares fitting of a straight line. *Can. J. Phys.,* **44,** 1079–1086.

Zhang, M. H., R. D. Cess, T. Y. Kwon, and M. H. Chen, 1994: Approaches of comparison for clear-sky radiative-fluxes from general circulation models with Earth Radiation Budget Experiment data. *J. Geophy. Res.,* **99,** 5515–5523.